Egyptian Journal of Chemistry

http://ejchem.journals.ekb.eg/

Synthesis, Characterization, and Adsorption Study of Magnetic Superhydrophobic Monolithic Core-Shell Polystyrene Composite for the Removal of Ethyl Naphthalene from Produced Water Using Fixed Column Bed

R. Hosny[1],*, Atef Mohamed Gad Mohamed[2], OH Abdelraheem[3], Modather F. Hussein[4,5],

Mahmoud F. Mubarak [6],*, Hanan A. Ahmed[7],*

[1]*Production Department, Egyptian Petroleum Research Institute, Nasr City, Cairo, Egypt*

[2]*Assiut and new valley company for water and wastewater fax No: 088229347, Assiut, Egypt*

[3]*Chemical Engineering Department, Faculty of Engineering, Beni-Suef University, Beni-Suef, Egypt*

[4]*Chemistry Department, College of Science, Jouf University, P.O. Box 2014, Sakaka, Aljouf, KSA*

[5]*Chemistry Department, Faculty of Science, Al-Azhar University, Assiut 71524, Egypt*

[6]*Petroleum Applications Department, Egyptian Petroleum Research Institute, Nasr City, Cairo, Egypt*

[7]*Petrochemicals Department, Egyptian Petroleum Research Institute, Nasr City, Cairo, Egypt*

_____

Abstract

This paper studies the removal of ethyl naphthalene as one of the polyaromatic hydrocarbon pollutants (PAHs) from the produced water. Magnetic super hydrophobic monolithic core-shell polystyrene (MSHMCSh@PS) was prepared using a simple and low-cost (facile in situ bulk radical polymerization) method, in the presence of 2-azobisisobutyronitrile as an initiator for ethyl naphthalene adsorption. The characterization of the MSHMCSh@PS was performed using FT-IR, TGA, SEM, TEM, and VSM. The possibility of PAHs adsorption from produced water was performed using the continuous adsorption study in a fixed-bed column. The effects of flow rate, concentration, and bed height were investigated. The results showed that the relationship between adsorption capacity with both inlet concentration and bed depth is a direct one, while the relationship between adsorption capacity and flow rate is an inverse relationship. The best column parameters were found at 2.5 ml/min flowing rate, 9 cm bed height, and 50 mg/L concentration. The experimental column results and the relationship between operating boundaries were analyzed according to Yoon-Nelson and Thomas models. The results indicated that the breakthrough curve follows the Yoon-Nelson model. The practical application results showed that the PAHs were adsorbed from the produced water using the prepared absorbent MSHMCSh@PS, which was distinguished by its superior ability.

Keywords: Synthesis and characterization; PAHs; Produced water treatment; Polystyrene; Magnetite; Adsorption

_____

1. Introduction

The wastewater generated from the ground to the surface during oil-gas production operations is known as the produced water (PW) and it's the largest byproduct volume on most offshore platforms [1-3]. Nearly 40% of PW is discharged into water bodies without being treated [4]. Various molecular weights polyaromatic hydrocarbons (PAHs), are stable and immune to biodegradation [5] and cause cancer in the lungs, bladder, and skin, as well as causing serious health problems in aquatic life when present at very low concentrations [6]. It is necessary to remove these pollutants before entering the environment with the help of appropriate methods [7, 8]. Consequently, crescent attention has been focused on developing suitable processes for their removal [9-12]. Compared with other PAH species, ethyl naphthalene is the simplest, most volatile; it has less toxicity and

_____

is easily found in the environment. In fact ethyl naphthalene has been used in several research laboratories and serves as a chemical model to develop catalysts and degradation process of PAHs [13-15]. Ethyl naphthalene (ENP) is known for being hydrophobic, flammable, highly volatile, and chemically stable in water media [16]. The environmental and health agencies have declared that the concentration of ENP in treated wastewater effluents should not exceed 0.059 mg/L [17]. There are several methods for treating water pollution including electrochemical treatment [18, 19], biofilm process [20], ozonation [21, 22], advanced oxidation processes [23, 24], and adsorption [25]. Among the various methods, adsorption is considered one of the most promising techniques in this regard especially for removing PAHs from the produced water [6, 26-28]. It is widely used by many research groups due to its high efficiency, simplicity, low-cost, reproducible and eco-friendly [29-33]. To remove the contaminants from water and wastewater, metal oxides, zeolites, and nano-particles were tested as promising materials [34-36]. Recently, ferrate (VI); the high valent iron, gained special interest due to its high redox potential [37]. Due to the low cost, high efficacy and environmentally friendly nature of ferrate (VI) oxidation method, it is considered a promising technique for removing organic pollutants [38, 39].

Monolithic adsorbents have been developed for use in bioseparation, catalysis, optics, and microfluidic [40, 41]. Such adsorbents have a continuous capacity for adsorption due to their morphological and physicochemical properties [42]. Their high separation efficiency is due to their permeability, excellent porous features, and low-pressure drop [43, 44]. Incorporating nanoparticles into monolithic matrices is the most effective modification process to solve the aforementioned challenges [45, 46]. Monoliths can be produced due to the copolymerization of some nanoparticles with appropriate monomers [40, 47]. Thus, monoliths are synthesized from nanoparticle doping via in situ polymerization or post-polymerization modifications that are imbued with the nanoparticle characteristics to improve their efficiency.

Nano-polystyrene with a regular hole is a tasteless and odorless plasticized synthetic polystyrene (PS) [48]. It is non-toxic, transparent, and clear and can sometimes be of a yellowish color. It loses its polymerization by heating to give monomers such as (methacrylate), which is molded at 100 °C. Consequently, it becomes molten and sticky at a temperature of 185 °C, as it is resistant to weak acids, bases, fatty alcohols, oils, greases, and waxes, but it is affected and dissolved by hydrocarbon compounds,

and this gives the advantages of use in the removal of light petroleum compounds such as ethyl naphthalene [49]. It has good water resistance and less water vapor resistance, high corrosion, and heat resistance.

Iron nanoparticles are particles smaller than micrometers from iron metal. It is characterized by being highly reactive due to its large outer surface area compared to its mass. It oxidizes rapidly to form free iron ions in the presence of oxygen and water. Magnetic iron nanocomposites in all forms are very widely used, such as in medical applications, treatment, and disinfection of drinking water, and it has also been used in the remediation of industrial wastewater polluted by organic halogen compounds and others [50-52].

The removal of ethyl naphthalene from oil-producing waters is to treat the produced water for management and reuse instead of seawater discharge that makes it easier for use in many areas, such as re-injecting and using in agriculture [53, 54]. The preparation of polystyrene in the monolithic configuration in the presence of a magnetic core gave the high adsorption characteristic and enhanced mesoporous surface properties against certain pollutants, which increases the adsorption selectivity toward ethyl naphthalene [55]. The dual function of the synthesized magnetic core-shell is due to the adsorption properties of the magnetic core against ethyl naphthalene in PW and its catalytic action of the monolithic composite polymer. Due to the surface adsorption of the core sell-by thick film of monolithic PS cover the Fe_3O_4. The synthesized monolithic core sell has core mesoporous holes that enhance the selective adsorption of ethyl naphthalene. The magnetic core has having a catalytic cracking action during the adsorption process that the regeneration process of MSHMCSh@PS (Fig. 1).
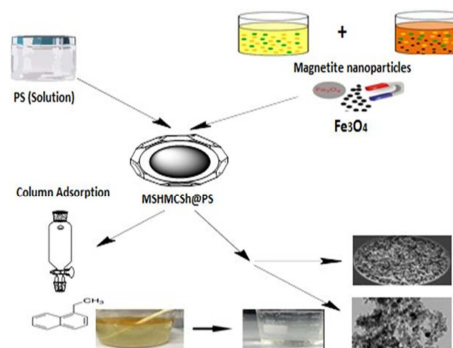
Figure 1: Adsorption process of ethyl naphthalene from produced water by magnetic superhydrophobic monolithic core-shell polystyrene (MSHMCSh@PS)

The majority of adsorption studies on ethyl naphthalene removal have been conducted in batch processes. Few research have attempted to investigate the adsorption performance in continuous flow columns. It is vital to perform further extended adsorption tests to cover pilot plant scales [26].

In this study, the main target is investigating the performance of a column packed with a newly developed, high-efficient, and easy-recyclable magnetic superhydrophobic monolithic core-shell polystyrene (MSHMCSh@PS) adsorbent for the removal of ethyl naphthalene from produced water. Firstly, magnetite (Fe$_3$O$_4$) nanoparticles were synthesized by the chemical co-precipitation method then, a magnetic core-shell polystyrene composite; (MSHMCSh@PS) was synthesized. Thereafter, the synthesized Fe$_3$O$_4$ and MSHMCSh@PS were fully characterized by FTIR, SEM, TEM, TGA, and VSM analysis. Based on the dynamic behavior of the fixed-bed column in terms of the breakthrough curve, the effects of bed depth, flow rate, and initial feed concentration on the removal of ethyl naphthalene by MSHMCSh@PS were studied. The experimental results were compared and discussed according to Yoon-Nelson and Thomas models.

2. Materials and Methods

2.1. Materials

Polystyrene (99% purity) and toluene (99% purity) were bought from Merck. Ferric chloride (FeCl$_3$·6H$_2$O, 99.99% purity) and ferrous chloride (FeCl$_2$·4H$_2$O, 99.99% purity) were bought from Fisher Scientific. Azobisisobutyronitrile (AIBN) initiator, sodium dodecyl sulfate (SDS), cetyltrimethylammonium bromide (CTAB), ammonia solution, NaOH, and ethanol were bought from Sinopharm Chemical Reagent Co., Ltd (Shanghai, China) and used without any further purification.

2.2. Methods
2.2.1. Synthesis of Fe$_3$O$_4$ Magnetic Core
Magnetic Fe$_3$O$_4$ nanoparticles were typically synthesized by the chemical co-precipitation method. 1.088 g of FeCl$_3$ (0.0067 mol) and 0.419 g (0.0033 mol) of FeCl$_2$ as Fe processor was added to 50 ml 0.03 mol/L mixture of 1:2 cationic surfactant (CTAB)/anionic surfactant (SDS) and kept to froze for 12 h. Such solution was gently shacked for 30 min, followed by mixing equal volumes of the two irons ions solutions, to obtain a solution containing a total Fe concentration of 0.1 mol/L, followed by adding 0.01 mol/L NaOH to adjust the pH value of the solution to 8. After more processes including

separation, precipitation, and drying, the Fe$_3$O$_4$ nanoparticles were calcinated at 550 °C/10 h (Fig. 2).
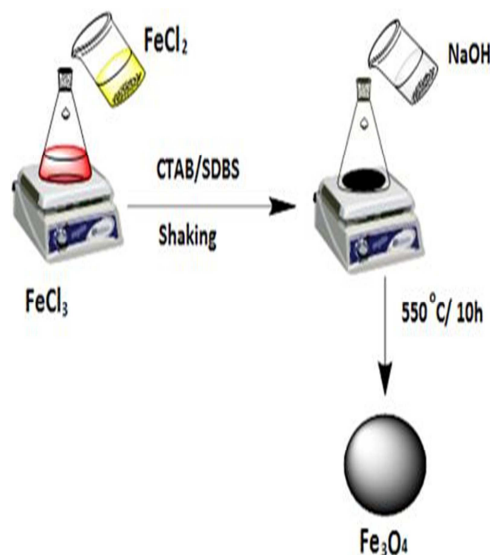
Figure 2: Synthesis of Fe$_3$O$_4$ Magnetic Core

2.2.2. Synthesis of Magnetic Superhydrophobic Monolithic Core-Shell Polystyrene (MSHMCSh@PS)
Five grams of styrene polymer were dissolved in toluene to obtain a well-dispersed suspension with a concentration of 25 wt%; for such dispersion, a 0.05 wt% of AIBN initiator was added to form a polymer solution, which in turn was transferred into a 250 ml flask. After that, twenty milliliters of 10 wt% aqueous CTAB solution were added and stirred for 2 h. The emulsion polymer solution was adjusted to pH 10 by adding 25 wt% ammonia aqueous solution. Then, the oil in water phases (styrene in toluene), was degassed by nitrogen gas for 20 min. The emulsion was transferred in vials and placed in the oven at 75 °C for 12 h. After complete polymerization, the vials were frozen and dried to get the porous PS monoliths. To obtain the magnetic superhydrophobic monolithic core-shell polystyrene, briefly, 20 ml of porous PS monoliths (0.1 mol) was quickly added to the support phase (gray mixture of Fe$_3$O$_4$ nanoparticles), and shake for 30 min using ultrasonic apparatus. The precipitate MSHMCSh@PS, wash with DW and ethanol several times, dried at 25 ºC/6 h in a vacuum oven, then calcinated at 550 ºC/6 h (Fig. 3).

_____
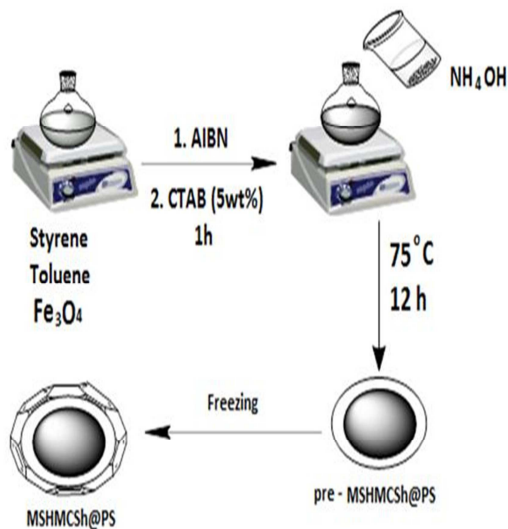
Figure 3: Synthesis of Magnetic Superhydrophobic Monolithic Core-Shell Polystyrene (MSHMCSh@PS)

2.3. Packed-Bed Adsorption Experiments

The initial ethyl naphthalene concentrations (10, 25, and 50 mg/L) were flowed individually through the column with a 2 cm inner diameter and a 50 cm height at a constant flow rate of 2.5, 5, and 10 ml/min. The column breakthrough is determined by measuring C/C_i (relation between the effluent MSHMCSh@PS concentration (C) to inlet MSHMCSh@PS concentration (Ci), whereas the total adsorbed concentrations (q) can be calculated from the difference between Ci and C, at a fixed time period [35, 36, 56]. The experiment was continued until the inlet and outlet ethyl naphthalene concentration became constant.

2.4. Desorption Experiments

To evaluate the purification of polluted water, the desorption and reusability study of adsorbent is an important issue to spot its ability to be reused and to restore its adsorption capacity. The reusability study of MSHMCSh@PS adsorbent is examined because it has been proposed as an adsorbent for the removal of ethyl naphthalene from produced water. The used MSHMCSh@PS nanocomposite was regenerated using a simple solvent-washing method. To desorb

ethyl naphthalene from MSHMCSh@PS nanocomposite, 0.025 g of used MSHMCSh@PS nanocomposite was mixed with 20 mL of ethanol and left for 1 h at 25 °C on a 350 rpm shaker water bath then filtered and dried for 2 h. After that the dried adsorbent was reused.

2.5. Modeling of the Breakthrough Curves

The efficiency of ethyl naphthalene adsorption onto MSHMCSh@PS, column performance, and the prediction of breakthrough curves were all detected using the Thomas model. Such a model supposes that the adsorption-desorption kinetics of the Langmuir process, and the rate of driven force, follow the second-order reversible reaction kinetics without affecting the axial distribution [57, 58]. Whereas Thomas's model can be written as the following:

$$\ln\left(\frac{C_o}{C} - 1\right) = \frac{k_{th} - q_o M}{F} - \frac{k_{th} - C_o V}{F} \qquad Eq\ (1)$$

where, C_0 is the influent MSHMCSh@PS concentration (mg/L), C is the effluent MSHMCSh@PS concentration (mg/L). Meanwhile, k_{th} (ml/min.mg) is the Thomas-constant, qo represents the equilibrium adsorption concentrations of ethyl naphthalene (mg/g), M symbolizes the mass of the adsorbent (g), and F indicates the flow rate (ml/min).

Yoon-Nelson simple model is designed for a single component system [59]. It doesn't require any detailed data on the characteristics of the absorbent, the physical properties of the adsorption bed, and the type of adsorbent because it's much less complicated than any other model. The Yoon-Nelson model assumes that the probability of adsorption decreases at a constant rate for each particle [60]. The Yoon-Nelson model is ineffective at predicting adsorption under a variety of conditions and obtaining the process variable. The Yoon-Nelson equation is shown in equation 2 below:

$$\ln\left(\frac{C}{C_o - C}\right) = k_{YN} t - t_{0.5} k_{YN} \qquad Eq\ (2)$$

where k_{YN} is the Yoon-Nelson rate constant, $t_{0.5}$ is the time taken for the 50% adsorbate to breakthrough the column, C_o and C is the initial and final concentration of the solution, respectively. In order to find out the value of k_{YN} and $t_{0.5}$, a graph of $\ln[C/(C_o-C)]$ against time needs to be plotted.

2.6. Characterization

FTIR spectroscopical analysis was done to confirm all samples structure using Nicolet IS-10 FTIR [61]. The surface morphology of the samples was carried out by scanning electron microscope (SEM, JEOL, JSM-6700F system) [61]. Transmission electron microscopy (TEM, Model JEM-200CX, Japan) was done for the samples to investigate their morphology [32]. The vibrating sample magnetometer (VSM, 7400-1, Lake Shore Co., Ltd., USA) cure analysis was also performed at 25 ºC in an applied field of 20 k0e to investigate the magnetic properties of the synthesized samples.

3. Results and Discussion

3.1. Characterizations

FTIR, TGA, SEM, TEM, and VSM measurements were used to characterize the various properties of the synthesized Fe_3O_4, and MSHMCSh@PS composite.

3.1.1. FTIR

FTIR spectra of ethyl naphthalene are present in Fig. 4 and exhibit C-C stretching vibration bands in the 1537-822 cm^{-1} range. In addition, a band appears at 3103–3005 cm^{-1} assigned for aromatic rings C-H stretching vibrations [62], while that band appeared at 2977 cm^{-1} region is due to C-H asymmetric and symmetric stretching vibrations of the methylene and methyl groups of C-substituents (Fig. 4) [63, 64].

Fig. 4 shows the FTIR spectra of ethyl naphthalene, polystyrene, Fe_3O_4, and MSHMCSh@PS. For PS the bands at 3384 and 3025 cm^{-1} represented the C–H aromatic stretching vibration, the stretching vibration at 2924 cm^{-1} for C–H, and the stretching vibration at 1679, 1453, 830, and 700 cm^{-1} represented the phenyl ring [63, 65, 66], where the typical absorption bands for polystyrene were clearly observed.

FTIR spectrums of Fe_3O_4 nanoparticles in Fig. 4 show three bands at 667, 1699, and 3457 cm^{-1}. The band at 580 cm^{-1} corresponds to the vibration of the Fe–O bonds in the crystalline lattice of Fe_3O_4 [67, 68].

All characteristic peaks of PS and Fe_3O_4 were observed in Fig. 4, reflecting the successful intercalating of Fe_3O_4 NPs into monolithic PS. The low intensity of Fe_3O_4 peaks with little shift

can be attributed to blending a low amount of Fe_3O_4 into the PS@ Fe_3O_4 monolithic beds. The bands at 1601 cm^{-1} of C=C of polystyrene stretching of MSHMCSh@PS, and 700–760 cm^{-1} revealed the monosubstituted benzene.
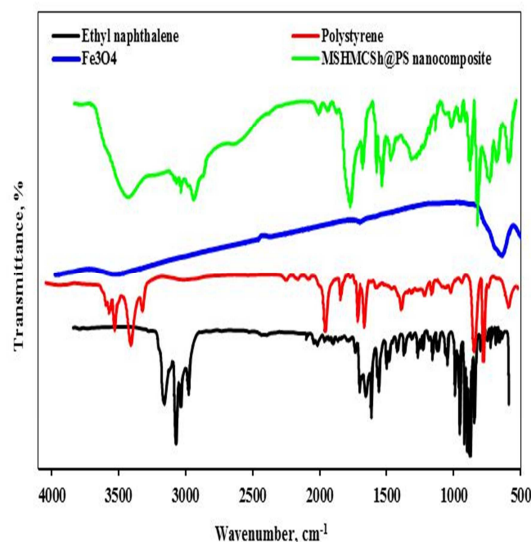
Figure 4: FTIR of ethyl naphthalene, polystyrene, Fe_3O_4 and MSHMCSh@PS

3.1.2. TGA

Fig. 5 illustrated the TGA for PS and exhibits two main mass loss steps presented at 338 °C and 426 °C due, respectively, to water removal and PS burning.

By temperature increasing from 300 °C to 600 °C there was no mass loss showing the existence of iron oxide only at this stage. In addition, the decomposition rate of the PS templates was slowed down after being protected by the Fe_3O_4 core. The first mass reduction phase occurred at 112–408 °C may indicate the PS structure destruction. The second step of mass reduction could have been caused by a rupture in the bonds in Fe_3O_4 nanoparticles recorded by numerous studies at temperatures above 800 °C [69].

In order to consider the sum of Fe_3O_4 in the heart of MSHMCSh@PS, there was a thermogravimetric study carried out. Fig. 5 shows the MSHMCSh@PS thermal decomposition diagrams synthesized by the green process. The findings show that bond breakup and weight loss occurred in only a few stages during the heating process in the nano-structures tested. PS, Fe_3O_4, and MSHMCSh@PS

curves are displayed in Fig. 5. Curve (a) reveals that the weight loss of nanocomposite by MSHMCSh@PS is between 42 °C and 950 °C around 4,9 percent, which is assigned with the weight loss of water as well as other usable molecules.

These composites suffer from chemical changes when heated due to the large entanglement that occurs between the polymer chains and the iron inside the core, and they become non-dissolving and incapable of melting at high temperatures, as is evident from Fig. 6. In addition to the elastomers (which are unsaturated hydrogen coals of high molecular weight that are characterized by the characteristic of elongation and their ability to expand and contract), these are properties inverse elasticity in the physical and mechanical properties of the polymer, such as specific size, heat capacity, specific heat, and elastic modulus.
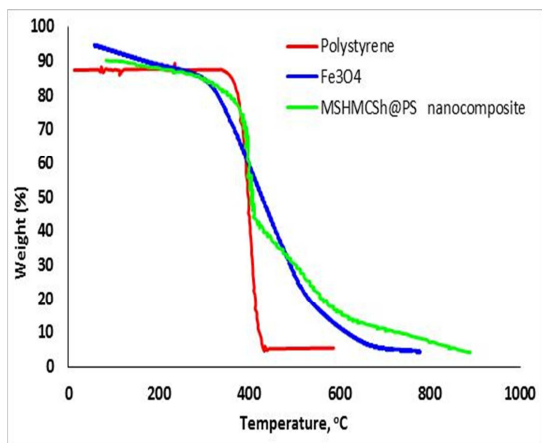
Figure 5: TGA analysis of polystyrene, Fe_3O_4, and MSHMCSh@PS

3.1.3.   SEM

The Fe_3O_4 and MSHMCSh@PS are shown in Fig. 6a and b for the image generation of a Scanning Electron Microscopy (SEM). According to the photos, we can see that the Fe_3O_4 nanoparticles are spherical and aggregation and agglomeration occur in some zones. Comparisons of photographs of MSHMCSh@PS and Fe_3O_4 show several pores as well as decreased aggregation and improved distribution of nanocomposite Fe_3O_4 nanoparticles. SEM images of MSHMCSh@PS adsorbent revealed irregular pore structure before adsorption and such

pores were filled with ethyl naphthalene after adsorption. Increasing the modified polystyrene sponge surface area can improve its adsorption capacity when exposed to magnetic fields of various strengths. Further increasing by addition of Fe_3O_4 nanoparticles will result in irregularly shaped particles with a broad size distribution (Fig. 6a). This is because that the Fe_3O_4 nanoparticles containing droplets affect the spatial distribution of the cross-linking density across the spheres and minimize the Gibbs interfacial free energy. Accordingly, the SEM images show that the microscopic spheres of magnetite particles are not homogeneous in shape and size but are circularly shaped.

Fig. 6b shows that the gray PS shell very well covers the dark magnetite particles. In addition, the magnetic properties of the modified PS sponge are conducive to magnet control and recycling. Thereby, it can be used for PAHs removal 15 times without reducing its adsorption capacity, while the exclusiveness of the super-hydrophobic functionalized PS sponge leads to selective removal from water. In addition, when connected to a peristaltic pump, the modified sponge can continuously collect ethyl naphthalene from the water.
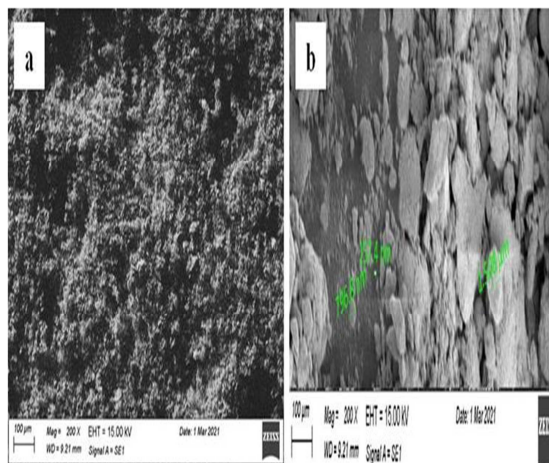
Figure 6: SEM images of a) Fe_3O_4 and b) MSHMCSh@PS composite

3.1.4.   TEM
The photographs of Fe_3O_4 and MSHMCSh@PS captured by the transmission electron microscope (TEM) are seen in Fig. 7a and b (TEM). The cubic

and circular structures in Fig. 7a are shown to be favorable to the stability of colloidal dispersion due to SDS ligands that were interconnected on the surface of Fe_3O_4 by O-S=O pairs. The typical nanostructural sizes are about 50 nm and 250 nm, respectively, based on the pictures. An increase in MSHMCSh@PS particle size has been identified in comparison with pure nanoparticles since polymerized nanoparticles and bonds are formed that prohibit nanoparticles and eventually nanocomposites from growing (Fig. 7b). The current research also conceives this kind of action, which resulted in increasing the prepared nanocomposite size of relative to the particles of pure iron oxide.

.
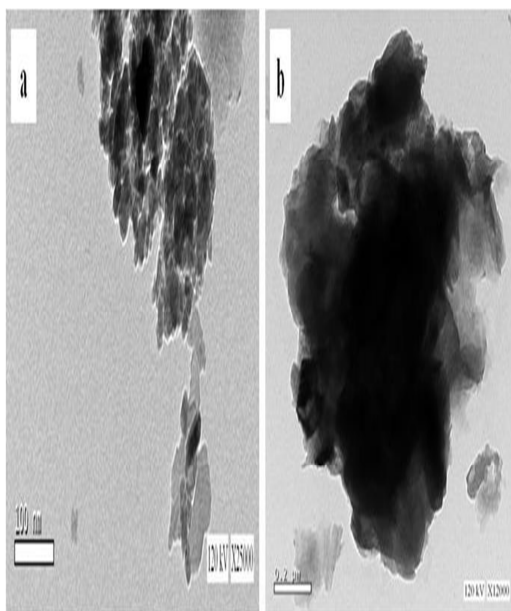
Figure 7: TEM of a) Fe_3O_4 and b) MSHMCSh@PS composite

3.1.5. VSM

The magnetization of Fe_3O_4 and MSHMCSh@PS composite was investigated and the results are shown in Fig. 8. As seen in Fig. 8, the Fe_3O_4 nanoparticles showed a high saturation magnetism (Ms) of 65 emu/g characterizing the superparamagnetic property of materials [70] however, the MSHMCSh@PS composite exhibited an Ms value of 55 emu/g which become lower as compared to Fe_3O_4 nanoparticles, due to the contribution of the non-magnetic polystyrene in the composition of the synthesized composite confirming its successful formation. The obtained results indicated that the synthesized

MSHMCSh@PS adsorbent can be easily separated by applying an external magnetic field after the adsorption process due to its excellent magnetic characteristics.
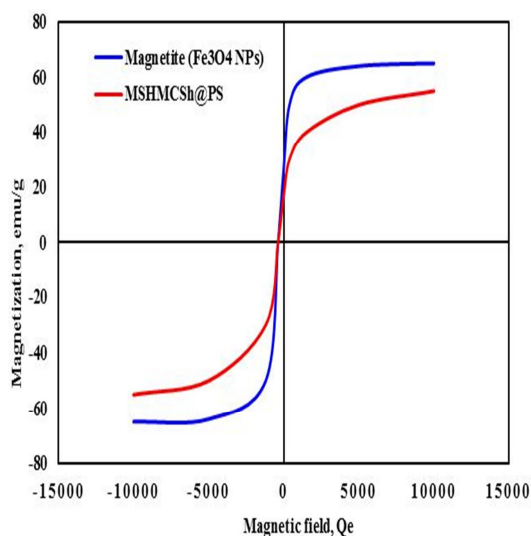
Figure 8: VSM curves of Fe_3O_4 and MSHMCSh@PS composite

3.2. Adsorption of Ethyl Naphthalene from Produced Water (PW) by Continuous Fixed-Bed Column study

3.2.1. Effect of Flow Rate

The breakthrough behavior of ethyl naphthalene at different flow rates was given in Fig. 9. The flow rate was changed in the range of 2.5, 5, and 10 ml/min, while the concentration of ethyl naphthalene in influent was kept constant at 50 mg/L. The obtained results show that the adsorption of ethyl naphthalene on the MSHMCSh@PS was strongly influenced by the flow rate. The results revealed that values of adsorption capacity decreased slightly when the flow rate increased.

From this figure, one can conclude that the best flow rate that achieved high removal efficiency and acceptable treated water volume is 2.5 ml/min. At a high flow rate, the uptake of ethyl naphthalene concentrations was decreased due to insufficient contact time for interacting the solute with the sorbent and the limited diffusivity of solute into the sportive sites or pores.
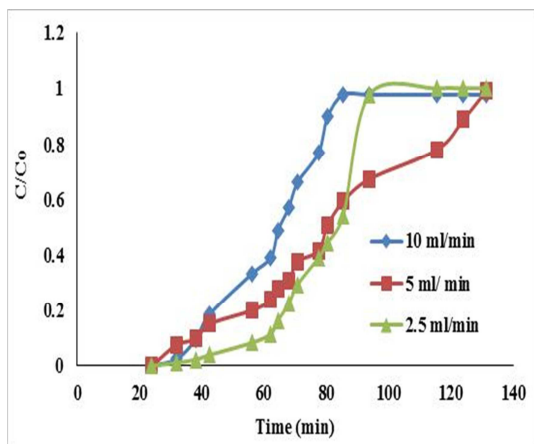
Figure 9: Breakthrough curve at different flow rates (Bed height= 9 cm and conc. =50 mg/L)

3.2.2. Effect of Bed Height

The breakthrough curves attained at different bed heights, constant influent concentration, and fixed flow rate that illustrated in Fig. 10 show, as the bed depth increased, the treated water volume and amount of ethyl naphthalene removal increased. It can be deduced that raising the bed depth up to 9 cm bed height increases the breakthrough time (t_b) and exhaustion time (t_e), perhaps owing to an increase in the surface area of the adsorbent and longer contact time. The higher bed height means more binding sites available.
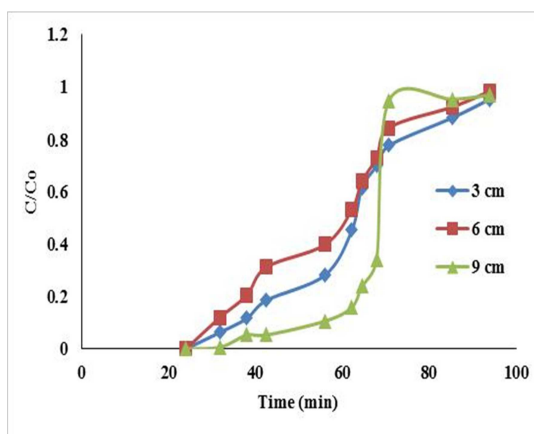
Figure 10: Breakthrough curve at different bed heights (Flow rate = 2.5 ml/min and conc. = 50 mg/L)

3.2.3. Effect of Concentration

The effect of initial ethyl naphthalene concentration on breakthrough curves in Fig. 11 was carried out at 10, 25, and 50 mg/L, as initial ethyl naphthalene, in the presence of 9 cm bed column height and at a 2.5 ml/min flow rate. The figure shows that as the initial concentration of ethyl naphthalene increases, both breakthrough time and exhaustion time decrease. At higher ethyl naphthalene concentrations of 50 mg/L, breakthrough curves were dispersed, and breakthroughs reached slowly. However, the values of qtotal and qe, were increased with increasing the inlet ethyl naphthalene concentration. Obviously, the moving of ethyl naphthalene moves to the surface of MSHMCSh@PS is very slow. Accordingly, it reduces all of the diffusion coefficients and driving forces of mass transfer. Therefore, the diffusion process depends on concentration [58, 71].
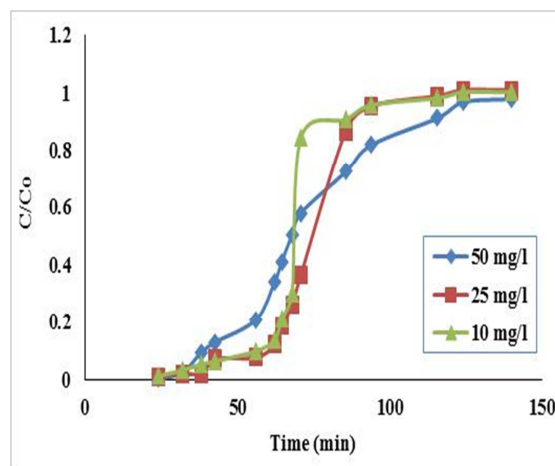
Figure 11: Breakthrough curve at different concentrations (Flow rate= 2.5 ml/min and bed height= 9 cm)

3.3. Breakthrough curve models

To estimate the breakthrough curves and to obtain the kinetic model of the column understudy, the fixed-bed column performance was described using two models (Thomas and Yoon-Nelson) Table 1. Comparisons of predicted models curve are shown in Figs. 12 and 13. Figures confirm that the expected Yoon-Nelson curve is nearer to investigational curves. Additionally, by applying two models as illustrated in Table 1, it is concluded that the correlation coefficient values R^2 of Thomas and Yoon - Nelson varied from 0.68 to 0.97 and 0.95 to 0.98, respectively. Clearly, that R^2 of the Yoon-Nelson model is higher than the Thomas model. Consequently, the Yoon-Nelson model is a well-fitted model for the ethyl naphthalene adsorption system.

Table 1. Thomas and Yoon-Nelson model parameters for ethyl naphthalene adsorption onto MSHMCSh@PS (Co = 50 mg/L, flow rate= 2.5 cm).

	Thomas Model			Yoon-Nelson		
	k_{Th}	q_0	R^2	k_{YN}	τ	R^2
Bed height						
3 cm	-2.62E-07	-6.38E-07	0.68293	0.00017	-29.041	0.95685
6 cm	1.70E-06	4.33E-06	0.68293	0.00016	-25.272	0. 97747
9 cm	1.08E-07	2.78E-08	0.97327	0.00012	-33.772	0.97108
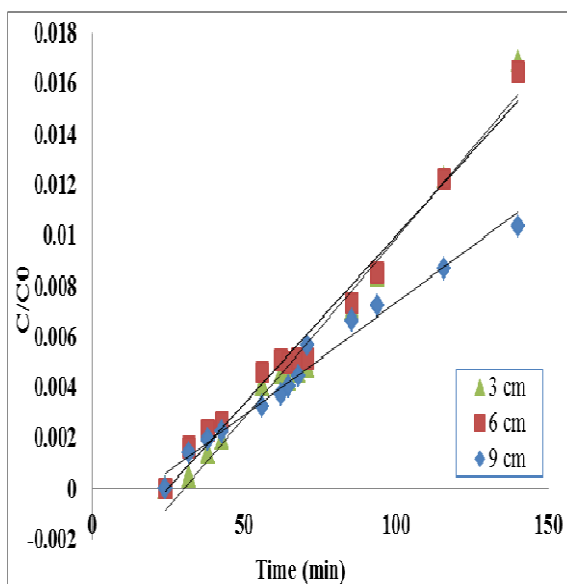
Figure 12: Thomas model for removal of ethyl naphthalene onto MSHMCSh@PS
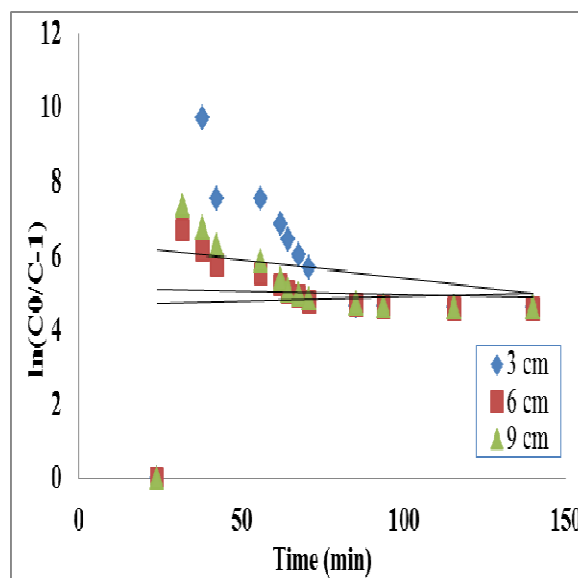
Figure 13: Yoon-Nelson model for removal of ethyl naphthalene onto

MSHMCSh@PS

3.4. Comparison of MSHMCSh@PS Adsorbent with Other Adsorbents Used for Ethyl Naphthalene Removal

As observed from Table 2, the synthesized MSHMCSh@PS magnetic composite was evaluated as easy-recyclable adsorbent for the removal of ethyl naphthalene from produced water and the obtained data are compared with the findings of other studies.

As shown, MSHMCSh@PS adsorbent is superior to most of the evaluated adsorbents as adsorbent for the removal of ethyl naphthalene in addition to its effective magnetic separation ability confirmed by the VSM results discussed above indicating the ability of its utilization as an environmentally friendly competitive adsorbent for PAHs removal from contaminated water especially ethyl naphthalene.

_____

Table 2. Removal of ethyl naphthalene from polluted water by various adsorbents

Adsorbent	Models	Maximum adsorption Capacity (mg/g)	Ref.
AC from petroleum	Freundlich isotherm	3.2	[72]
AC from coal tar pitch/furfural	Langmuir isotherm	18.75	[73]
AC from wood waste	Temkin isotherm	22.33	[74]
Single CNTs	Langmuir isotherm	81.18	[75]
Multiwalled CNTs	Dubinin – Astakhov isotherm	49.0	[76]
Graphene oxide from rice straw	Langmuir isotherm	3.33	[77]
clay	Langmuir, Freundlich and	39.84	[78]
sandy soil	Tempkin isotherms	19.92	
Hydroxyapatite	Freundlich isotherm	12.9 3	[79]
Surfactant-modified mesoporous silica	Temkin isotherm	2.60	[80]
Waste tyre Langmuir isotherm	Langmuir isotherm	21.74	[81]
Sugarcane bagasse	Langmuir	3.73	[82]
Kaolin/Fe_3O_4 composite	Freundlich	1.70	[83]
AC/Fe_3O_4 composite	Langmuir isotherm	120.87	[84]
SDS-encapsulated chitosan beads	Chapman sigmoidal isotherm	28.66	[85]
Magnetic polystyrene (MSHMCSh@PS)	Yoon-Nelson model	46.9	Current Study

Note that: AC is the activated carbon, CNTs is the carbon nanotubes, and SDS is sodium dodecyl sulfate

3.5. Desorption Study

To determine the stability, feasibility and better performance of the synthesized MSHMCSh@PS adsorbent, the removal efficiency of ethyl naphthalene was studied after four adsorption/desorption cycles with ethanol as desorbing agent and the results are shown in Fig. 14. After four adsorption/desorption cycles, the ethyl naphthalene removal efficiency has shown a slight decrease due to the slight decrease in the activity of the adsorbent surface active sites. The removal efficiency has reached ~ 90% after 4 cycles which indicates that the ethanol-washing approach was successful in renewing the MSHMCSh@PS composite and confirming the stability and good performance of the synthesized MSHMCSh@PS adsorbent.
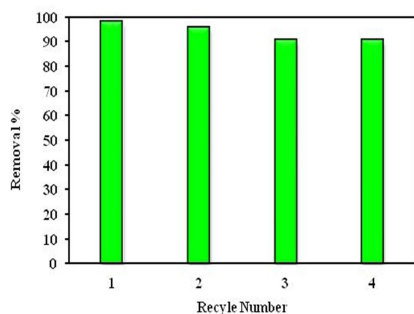
Figure 14: The reproducibility results of MSHMCSh@PS composite toward ethyl naphthalene removal

4. Conclusion

This article synthesizes and then uses nanocomposite MSHMCSh@PS to experiment in columns to treat PW for reuse instead of seawater discharge. FTIR, TGA, SEM, and TEM are the composite characteristics. Based on the experimental findings obtained from column tests, it is concluded that it is an effective and viable approach to remove ethyl naphthalene from a packaged bed system using MSHMCSh@PS. In addition, the adsorption depends on the bed depth, the influential concentration of ethyl naphthalene and the flow rate. The adsorption mechanism increases with the bed's height, and the overall weights of ethyl naphthalene adsorbed by a monolithic composite of MSHMCSh@PS are also raised in the column. The maximum column potential was determined at a flow rate of 2.5 ml/min, a concentration of 50 mg/L, and a bed height of 9 cm. The Yoon-Nelson a model can be used to describe the behavior of breakthrough curves. In addition, such model is the best model to predict the entire breakthrough curve, also is the simplest way to forecast the complete breakthrough curve. Finally, it was clear that with the use of the prepared nanocomposite MSHMCSh@PS, it could increase the volume of production of the treated wastewater "produced water" with high selectivity of organic pollutants and manage it for reuse again.

_____

5. Conflict of Interest

The authors declare that they have no conflict of interest to declare.

6. Funding

7. Acknowledgments

8. References

[1] Hosny R., Fathy M., Ramzi M., Abdel Moghny T., Desouky S.E.M., Shama S.A., Treatment of the oily produced water (OPW) using coagulant mixtures, Egyptian Journal of Petroleum 25(3) (2016) 391-396. doi: https://doi.org/10.1016/j.ejpe.2015.09.006.

[2] Kassab M.A., Abbas A.E., Elgamal I., Shawky B.M., Mubarak M.F., Hosny R., Review on the Estimating the Effective Way for Managing the Produced Water: Case Study, Open Journal of Modern Hydrology 11(2) 19-37. doi:

[3] Al-Mhyawi S.R., Mubarak M.F., Hosny R., Amine M., Abdelraheem O.H., Zayed M.A., Ragab A.H., El Shahawy A., Enhanced Nanofiltration Process of Thin Film Composite Membrane Using Dodecyl Phenol Ethoxylate and Oleic Acid Ethoxylate for Oilfield Calcite Scale Control, Membranes 11(11) (2021) 855. doi: 10.3390/membranes11110855.

[4] Jiménez S., Micó M., Arnaldos M., Medina F., Contreras S., State of the art of produced water treatment, Chemosphere 192 (2018) 186-208. doi:

[5] Govarthanan M., Khalifa A.Y., Kamala-Kannan S., Srinivasan P., Selvankumar T., Selvam K., Kim W., Significance of allochthonous brackish water Halomonas sp. on biodegradation of low and high molecular weight polycyclic aromatic hydrocarbons, Chemosphere 243 (2020) 125389. doi:

[6] Al-Ghouti M.A., Al-Kaabi M.A., Ashfaq M.Y., Da'na D.A., Produced water characteristics, treatment and reuse: A review, Journal of Water Process Engineering 28 (2019) 222-239. doi:

[7] Gan Y., Ding C., Xu B., Liu Z., Zhang S., Cui Y., Wu B., Huang W., Song X., Antimony (Sb) pollution control by coagulation and membrane filtration in water/wastewater treatment: A comprehensive review, Journal of Hazardous Materials 442 (2023) 130072. doi: 10.1016/j.jhazmat.2022.130072.

[8] Sadia M., Mahmood A., Ibrahim M., Irshad M.K., Quddusi A.H.A., Bokhari A., Mubashir M., Chuah L.F., Show P.L., Microplastics pollution from wastewater treatment plants: A critical review on challenges, detection, sustainable removal techniques and circular economy, Environmental Technology & Innovation 28 (2022) 102946. doi: 10.1016/j.eti.2022.102946.

[9] Lamichhane S., Krishna K.B., Sarukkalige R., Polycyclic aromatic hydrocarbons (PAHs) removal by sorption: a review, Chemosphere 148 (2016) 336-353. doi:

[10] Eeshwarasinghe D., Loganathan P., Kalaruban M., Sounthararajah D.P., Kandasamy J., Vigneswaran S., Removing polycyclic aromatic hydrocarbons from water using granular activated carbon: kinetic and equilibrium adsorption studies, Environmental Science and Pollution Research 25(14) (2018) 13511-13524. doi: 10.1007/s11356-018-1518-0.

[11] Makkar R.S., Rockne K.J., Comparison of synthetic surfactants and biosurfactants in enhancing biodegradation of polycyclic aromatic hydrocarbons, Environmental Toxicology and Chemistry: An International Journal 22(10) (2003) 2280-2292. doi:

[12] Navarro R.R., Iimura Y., Ichikawa H., Tatsumi K., Treatment of PAHs in contaminated soil by extraction with aqueous DNA followed by biodegradation with a pure culture of Sphingomonas sp, Chemosphere 73(9) (2008) 1414-1419. doi:

[13] Aranda A., López J.M., Murillo R., Mastral A.M., Dejoz A., Vázquez I., Solsona B., Taylor S.H., García T., Total oxidation of naphthalene with high selectivity using a ceria catalyst prepared by a combustion method employing ethylene glycol, Journal of Hazardous Materials 171(1-3) (2009) 393-399. doi: 10.1016/j.jhazmat.2009.06.013.

[14] Chang C.-F., Chang C.-Y., Chen K.-H., Tsai W.-T., Shie J.-L., Chen Y.-H., Adsorption of naphthalene on zeolite from aqueous solution, J. Colloid Interface Sci. 277(1) (2004) 29-34. doi: 10.1016/j.jcis.2004.04.022.

[15] Karimi B., Habibi M., Esvand M., Biodegradation of naphthalene using Pseudomonas aeruginosa by up flow anoxic-aerobic continuous flow combined bioreactor, J Environ Health Sci Eng 13 (2015) 26-26. doi: 10.1186/s40201-015-0175-1.

[16] Ghaedi M., Daneshyar A., Asfaram A., Purkait M.K., Adsorption of naphthalene onto high-surface-area nanoparticle loaded activated carbon by high performance liquid chromatography: response surface methodology, isotherm and kinetic study, RSC Advances 6(59) (2016) 54322-54330. doi: 10.1039/c6ra09500c.

[17] Mijaylova Nacheva P., Esquivel Sotelo A., Removal of naphthalene and phenanthrene using aerobic membrane bioreactor, Biodegradation 27(2-3) (2016) 83-93. doi: 10.1007/s10532-016-9757-6.

[18] Leng Q., Xu S., Wu X., Wang S., Jin D., Wang P., Wu D., Dong F., Electrochemical removal of synthetic methyl orange dyeing wastewater by reverse electrodialysis reactor: Experiment and mineralizing model, Environ. Res. 214 (2022) 114064. doi: 10.1016/j.envres.2022.114064.

[19] Sarfo D.K., Kaur A., Marshall D.L., O'Mullane A.P., Electrochemical degradation and mineralisation of organic dyes in aqueous nitrate solutions, Chemosphere 316 (2023) 137821. doi: 10.1016/j.chemosphere.2023.137821.

_____

_____

[20] Cheng Z., Chen Z., Li J., Zuo S., Yang P., Mesoporous silica-pillared clays supported nanosized Co3O4-CeO2 for catalytic combustion of toluene, Applied Surface Science 459 (2018) 32-39. doi: 10.1016/j.apsusc.2018.07.203.

[21] Cui B., Fu S., Hao X., Zhou D., Synergistic effects of simultaneous coupling ozonation and biodegradation for coking wastewater treatment: Advances in COD removal, toxic elimination, and microbial regulation, Chemosphere 318 (2023) 137956. doi: 10.1016/j.chemosphere.2023.137956.

[22] Elsayed I., Madduri S., El-Giar E.M., Hassan E.B., Effective removal of anionic dyes from aqueous solutions by novel polyethylenimine-ozone oxidized hydrochar (PEI-OzHC) adsorbent, Arabian Journal of Chemistry 15(5) (2022) 103757. doi: 10.1016/j.arabjc.2022.103757.

[23] El Gaidoumi A., Arrahli A., Loqman A., Baragh F., El Bali B., Kherbeche A., Efficient Sol-gel Nanocomposite TiO2-clay in Photodegradation of Phenol: Comparison to Labe-made and Commercial Photocatalysts, Silicon 14(10) (2021) 5401-5414. doi: 10.1007/s12633-021-01275-1.

[24] Gaidoumi A.E., Benabdallah A.C., Bali B.E., Kherbeche A., Synthesis and Characterization of Zeolite HS Using Natural Pyrophyllite as New Clay Source, Arabian Journal for Science and Engineering 43(1) (2017) 191-197. doi: 10.1007/s13369-017-2768-8.

[25] Adebayo M.A., Areo F.I., Removal of phenol and 4-nitrophenol from wastewater using a composite prepared from clay and Cocos nucifera shell: Kinetic, equilibrium and thermodynamic studies, Resources, Environment and Sustainability 3 (2021) 100020. doi: 10.1016/j.resenv.2021.100020.

[26] Alshabib M., Removal of naphthalene from wastewaters by adsorption: a review of recent studies, Int. J. Environ. Sci. Technol. (Tehran) 19(5) (2021) 4555-4586. doi: 10.1007/s13762-021-03428-6.

[27] Chowdhury S., Balasubramanian R., Recent advances in the use of graphene-family nanoadsorbents for removal of toxic pollutants from wastewater, Adv. Colloid Interface Sci. 204 (2014) 35-56. doi: 10.1016/j.cis.2013.12.005.

[28] Ahmed A.M., Hosny R., Mubarak M.F., Younes A.A., Farag A.B., Green magnetic clay nanocomposite based on graphene oxide nanosheet as a synthetic low-cost adsorbent for oil droplets removal from produced water, Desalination and Water Treatment 280 (2022) 206-223. doi: 10.5004/dwt.2022.29031.

[29] Gupta K., Khatri O.P., Fast and efficient adsorptive removal of organic dyes and active pharmaceutical ingredient by microporous carbon: Effect of molecular size and charge, Chemical Engineering Journal 378 (2019) 122218. doi: 10.1016/j.cej.2019.122218.

[30] Zhang Y., Li K., Liao J., Facile synthesis of reduced-graphene-oxide/rare-earth-metal-oxide aerogels as a highly efficient adsorbent for Rhodamine-B, Applied Surface Science 504 (2020) 144377. doi: 10.1016/j.apsusc.2019.144377.

[31] Ahmed H.A., Mubarak M.F., Adsorption of Cationic Dye Using A newly Synthesized CaNiFe2O4/Chitosan Magnetic Nanocomposite: Kinetic and Isotherm Studies, J. Polym. Environ. 29(6) (2021) 1835-1851. doi: 10.1007/s10924-020-01989-0.

[32] Ahmed H.A., Soliman M.S.S., Othman S.A., Synthesis and Characterization of Magnetic Nickel Ferrite-Modified Montmorillonite Nanocomposite For Cu (II) and Zn (II) Ions Removal From Wastewater, Egyptian Journal of Chemistry 0(0) (2021) 0-0. doi: 10.21608/ejchem.2021.69597.3527.

[33] Yan Y., Yuvaraja G., Liu C., Kong L., Guo K., Reddy G.M., Zyryanov G.V., Removal of Pb(II) ions from aqueous media using epichlorohydrin crosslinked chitosan Schiff's base@Fe3O4 (ECCSB@Fe3O4), Int. J. Biol. Macromol. 117 (2018) 1305-1313. doi: 10.1016/j.ijbiomac.2018.05.204.

[34] El-Sayed M.E., Nanoadsorbents for water and wastewater remediation, Science of The Total Environment (2020) 139903. doi:

[35] El-Maghrabi H.H., Hosny R., Ramzi M., Zayed M.A., Fathy M., Preparation and Characterization of Novel Magnetic ZnFe2O4–Hydroxyapatite Core–Shell Nanocomposite and Its Use as Fixed Bed Column System for Removal of Oil Residue in Oily Wastewater Samples, Egyptian Journal of Petroleum 28(2) (2019) 137-144. doi: https://doi.org/10.1016/j.ejpe.2018.12.005.

[36] El-Maghrabi H.H., Hosny R., Ramzi M., Abdou M., Fathy M., Novel mesoporous silica (MCM-41) and its characterization for oil adsorption from produced water injected in water injection projects using fixed bed column processes (vol 60, 70, 2017), Desalination and Water Treatment 119 (2018) 284-284. doi:

[37] Haneef T., Mustafa M.R.U., Wan Yusof K., Isa M.H., Bashir M.J., Ahmad M., Zafar M., Removal of Polycyclic Aromatic Hydrocarbons (PAHs) from Produced Water by Ferrate (VI) Oxidation, Water 12(11) (2020) 3132. doi:

[38] Ali I., Asim M., Khan T.A., Low cost adsorbents for the removal of organic pollutants from wastewater, Journal of environmental management 113 (2012) 170-183. doi:

[39] Mubarak M.F., Ragab A.H., Hosny R., Ahmed I.A., Ahmed H.A., El-Bahy S.M., El Shahawy A., Enhanced performance of chitosan via a novel quaternary magnetic nanocomposite chitosan/grafted halloysitenanotubes@ ZnÎ³Fe3O4 for Uptake of Cr (III), Fe (III), and Mn (II) from Wastewater, Polymers 13(16) 2714. doi:

[40] Acquah C., Obeng E.M., Agyei D., Ongkudon C.M., Moy C.K., Danquah M.K., Nano-doped monolithic materials for molecular separation, Separations 4(1) (2017) 2. doi:

[41] Szumski M., Kłodzińska E., Jarmalavičienė R., Maruška A., Buszewski B., Considerations on influence of charge distribution on determination

_____

of biomolecules and microorganisms and tailoring the monolithic (continuous bed) materials for bioseparations, Journal of biochemical and biophysical methods 70(1) (2007) 107-115. doi:

[42] Arrua R.D., Strumia M.C., Alvarez Igarzabal C.I., Macroporous Monolithic Polymers: Preparation and Applications, Materials 2(4) (2009) 2429-2466. doi: 10.3390/ma2042429.

[43] Wang B., Prinsen P., Wang H., Bai Z., Wang H., Luque R., Xuan J., Macroporous materials: microfluidic fabrication, functionalization and applications, Chemical Society Reviews 46(3) (2017) 855-914. doi:

[44] 楊卓航, Functional Cellulose Monoliths for Flow-Based Applications, (2020). doi:

[45] Fresco-Cala B., Cárdenas S., Potential of nanoparticle-based hybrid monoliths as sorbents in microextraction techniques, Analytica chimica acta 1031 (2018) 15-27. doi:

[46] Connolly D., Currivan S., Paull B., Polymeric monolithic materials modified with nanoparticles for separation and detection of biomolecules: a review, Proteomics 12(19-20) (2012) 2904-2917. doi:

[47] Fresco-Cala B., Mompó-Roselló Ó., Simó-Alfonso E.F., Cárdenas S., Herrero-Martínez J.M., Carbon nanotube-modified monolithic polymethacrylate pipette tips for (micro) solid-phase extraction of antidepressants from urine samples, Microchimica Acta 185(2) (2018) 1-7. doi:

[48] Arabi A.M., Ebadzadeh T., Yousefi A.A., Pishvaei M., MARZBAN R.E., Najafi F., The function of nano-polystyrene template and comb polycarboxylic acid surfactant in synthesis of ZnS nanoparticles via hydrothermal method, (2011). doi:

[49] Manea M., Kirmaier L., Sander J., 4. Organic coating materials, Anticorrosive Coatings, Vincentz Network2014, pp. 37-98.

[50] Ahmed H.A., Mubarak M.F., Adsorption of Cationic Dye Using A newly Synthesized CaNiFe2O4/Chitosan Magnetic Nanocomposite: Kinetic and Isotherm Studies, J. Polym. Environ. 29(6) (2021) 1835-1851. doi: 10.1007/s10924-020-01989-0.

[51] Ahmed H.A., Soliman M.S.S., Othman S.A., Synthesis and Characterization of Magnetic Nickel Ferrite-Modified Montmorillonite Nanocomposite For Cu (II) and Zn (II) Ions Removal From Wastewater, Egypt J Chem 64(0) (2021) 56270-5645. doi: 10.21608/ejchem.2021.69597.3527.

[52] Mubarak M.F., Ragab A.H., Hosny R., Ahmed I.A., Ahmed H.A., El-Bahy S.M., El Shahawy A., Enhanced Performance of Chitosan via a Novel Quaternary Magnetic Nanocomposite Chitosan/Grafted Halloysitenanotubes@ZnγFe(3)O(4) for Uptake of Cr (III), Fe (III), and Mn (II) from Wastewater, Polymers 13(16) (2021) 2714. doi: 10.3390/polym13162714.

[53] Silva T.L., Morales-Torres S., Castro-Silva S., Figueiredo J.L., Silva A.M., An overview on exploration and environmental impact of unconventional gas sources and treatment options for produced water, Journal of environmental management 200 (2017) 511-529. doi:

[54] Varonka M.S., Gallegos T.J., Bates A.L., Doolan C., Orem W.H., Organic compounds in produced waters from the Bakken Formation and Three Forks Formation in the Williston Basin, North Dakota, Heliyon 6(3) (2020) e03590. doi:

[55] Du Z., Deng S., Bei Y., Huang Q., Wang B., Huang J., Yu G., Adsorption behavior and mechanism of perfluorinated compounds on various adsorbents—A review, Journal of hazardous materials 274 (2014) 443-454. doi:

[56] Ibrahim T.H., Sabri M.A., Khamis M.I., Application of multiwalled carbon nanotubes and its magnetite derivative for emulsified oil removal from produced water, Environmental technology 40(25) (2019) 3337-3350. doi:

[57] Atar N., Olgun A., Wang S., Liu S., Adsorption of Anionic Dyes on Boron Industry Waste in Single and Binary Solutions Using Batch and Fixed-Bed Systems, Journal of Chemical & Engineering Data 56(3) (2011) 508-516. doi: 10.1021/je100993m.

[58] Futalan C.M., Kan C.-C., Dalida M.L., Pascua C., Wan M.-W., Fixed-bed column studies on the removal of copper using chitosan immobilized on bentonite, Carbohydrate polymers 83(2) (2011) 697-704. doi:

[59] Vera L.M., Bermejo D., Uguña M.F., Garcia N., Flores M., González E., Fixed bed column modeling of lead (II) and cadmium (II) ions biosorption on sugarcane bagasse, Environmental Engineering Research 24(1) (2019) 31-37. doi:

[60] Karri R.R., Sahu J., Jayakumar N., Optimal isotherm parameters for phenol adsorption from aqueous solutions onto coconut shell based activated carbon: error analysis of linear and non-linear methods, Journal of the Taiwan Institute of Chemical Engineers 80 (2017) 472-487. doi:

[61] Ahmed H.A., Elbanna S.A., Khalil R., Tayel A., El Basaty A.B., Ultrasonic-assisted Hydrothermal Synthesis of Zeolite Y Adsorbent from Natural Kaolin for the Recycling of Waste Engine Oil, Egyptian Journal of Chemistry 65(13) (2022) -. doi: 10.21608/ejchem.2022.106134.4879.

[62] Elbanna S.A., Abd El Rhman A.M.M., Al-Hussaini A.S., Khalil S.A., Synthesis, characterization, and performance evaluation of novel terpolymers as pour point depressors and paraffin inhibitors for Egyptian waxy crude oil, Petroleum Science and Technology 40(18) (2022) 2263-2283. doi: 10.1080/10916466.2022.2041660.

[63] Elbanna S.A., Abd El Rhman A.M.M., Al-Hussaini A.S., Khalil S.A., Paraffin inhibition and pour point depression of waxy crude oil using newly synthesized terpolymeric additives, Egyptian Journal of Chemistry (2022) -. doi: 10.21608/ejchem.2022.132291.5838.

[64] Hanafi S.A., Elmelawy M.S., Ahmed H.A., Solvent-free deoxygenation of low-cost fat to produce diesel-like hydrocarbons over Ni–MoS2/Al2O3–TiO2 heterogenized catalyst, International Journal of Energy and Water

_____

Resources 6(1) (2021) 1-13. doi: 10.1007/s42108-021-00156-y.

[65] Elbanna S.A., Ahmed H.A., Bioresoursed Nano-SiO2/Styrene-Co-Vinyl Acetate Nano-Composite: Synthesis, Characterization and Evaluation as Nano-Pour Point Depressant and Paraffin Inhibitor for Waxy Crude Oil, Egyptian Journal of Chemistry (2023) -. doi: 10.21608/ejchem.2023.181813.7351.

[66] Elbanna S.A., Abd El Rhman A.M.M., Al-Hussaini A.S., Khalil S.A., Development of Novel Terpolymes and Evaluating Their Performance as Pour Point Depressants and Paraffin Inhibitors for Waxy Crude Oil, Egyptian Journal of Chemistry (2022) -. doi: 10.21608/ejchem.2022.120528.5414.

[67] Ahmed H.A., Soliman M.S.S., Othman S.A., Synthesis and Characterization of Magnetic Nickel Ferrite-Modified Montmorillonite Nanocomposite For Cu (II) and Zn (II) Ions Removal From Wastewater, Egypt. J. Chem. 0(0) (2021) 0-0. doi: 10.21608/ejchem.2021.69597.3527.

[68] Deyab M.A., Awadallah A.E., Ahmed H.A., Mohsen Q., Progress study on nickel ferrite alloy-graphene nanosheets nanocomposites as supercapacitor electrodes, Journal of Energy Storage 46 (2022) 103926. doi: 10.1016/j.est.2021.103926.

[69] Asghar M.A., Zahir E., Asghar M.A., Iqbal J., Rehman A.A., Facile, one-pot biosynthesis and characterization of iron, copper and silver nanoparticles using Syzygium cumini leaf extract: As an effective antimicrobial and aflatoxin B1 adsorption agents, PloS one 15(7) (2020) e0234964. doi:

[70] Tabar Maleki S., Sadati S.J., Synthesis and investigation of hyperthermia properties of Fe3O4/HNTs magnetic nanocomposite, Inorg. Chem. Commun. 145 (2022) 110000. doi: 10.1016/j.inoche.2022.110000.

[71] Han Q., Chen Y., Wang Z., A generic two-band model for unconventional superconductivity and spin-density-wave order in electron-and hole-doped iron-based superconductors, EPL (Europhysics Letters) 82(3) (2008) 37007. doi:

[72] Yuan M., Tong S., Zhao S., Jia C.Q., Adsorption of polycyclic aromatic hydrocarbons from water using petroleum coke-derived porous carbon, Journal of Hazardous Materials 181(1-3) (2010) 1115-1120. doi: 10.1016/j.jhazmat.2010.05.130.

[73] Cabal B., Budinova T., Ania C.O., Tsyntsarski B., Parra J.B., Petrova B., Adsorption of naphthalene from aqueous solution on activated carbons obtained from bean pods, Journal of Hazardous Materials 161(2-3) (2009) 1150-1156. doi: 10.1016/j.jhazmat.2008.04.108.

[74] Barman S.R., Banerjee P., Das P., Mukhopadhayay A., Urban wood waste as precursor of activated carbon and its subsequent application for adsorption of polyaromatic hydrocarbons, International Journal of Energy and Water Resources 2(1-4) (2018) 1-13. doi: 10.1007/s42108-018-0001-4.

[75] Moradi O., Yari M., Moaveni P., Norouzi M., Removal of p-nitrophenol and Naphthalene from

Petrochemical Wastewater Using SWCNTs and SWCNT-COOH Surfaces, Fullerenes, Nanotubes and Carbon Nanostructures 20(1) (2012) 85-98. doi: 10.1080/1536383x.2010.533309.

[76] Wu W., Chen W., Lin D., Yang K., Influence of Surface Oxidation of Multiwalled Carbon Nanotubes on the Adsorption Affinity and Capacity of Polar and Nonpolar Organic Compounds in Aqueous Phase, Environmental Science & Technology 46(10) (2012) 5446-5454. doi: 10.1021/es3004848.

[77] Das P., Goswami S., Maiti S., Removal of naphthalene present in synthetic waste water using novel Graphene /Graphene Oxide nano sheet synthesized from rice straw: comparative analysis, isotherm and kinetics, Frontiers in Nanoscience and Nanotechnology 2(1) (2016). doi: 10.15761/fnn.1000107.

[78] Osagie E.I., Owabor C.N., Adsorption of Naphthalene on Clay and Sandy Soil from Aqueous Solution, Advances in Chemical Engineering and Science 05(03) (2015) 345-351. doi: 10.4236/aces.2015.53036.

[79] Bouiahya K., Oulguidoum A., Laghzizil A., Shalabi M., Nunzi J.M., Masse S., Hydrophobic chemical surface functionalization of hydroxyapatite nanoparticles for naphthalene removal, Colloids and Surfaces A: Physicochemical and Engineering Aspects 595 (2020) 124706. doi: 10.1016/j.colsurfa.2020.124706.

[80] Vidal C.B., Barros A.L., Moura C.P., de Lima A.C.A., Dias F.S., Vasconcellos L.C.G., Fechine P.B.A., Nascimento R.F., Adsorption of polycyclic aromatic hydrocarbons from aqueous solutions by modified periodic mesoporous organosilica, J. Colloid Interface Sci. 357(2) (2011) 466-473. doi: 10.1016/j.jcis.2011.02.013.

[81] Aisien F.A., Amenaghawon A.N., Adinkwuye A.I., Batch study, equilibrium and kinetics of adsorption of naphthalene using waste tyre rubber granules, Journal of Xenobiotics 4(1) (2014). doi: 10.4081/xeno.2014.2264.

[82] Younis S.A., El-Gendy N.S., El-Azab W.I., Moustafa Y.M., Kinetic, isotherm, and thermodynamic studies of polycyclic aromatic hydrocarbons biosorption from petroleum refinery wastewater using spent waste biomass, Desalination and Water Treatment (2014) 1-11. doi: 10.1080/19443994.2014.964331.

[83] Arizavi A., Mirbagheri N.S., Hosseini Z., Chen P., Sabbaghi S., Efficient removal of naphthalene from aqueous solutions using a nanoporous kaolin/Fe3O4 composite, Int. J. Environ. Sci. Technol. (Tehran) 17(4) (2019) 1991-2002. doi: 10.1007/s13762-019-02521-1.

[84] Kumar J.A., Amarnath D.J., Narendrakumar G., Anand K.V., Optimization of process parameters for naphthalene removal onto nano-iron oxide/carbon composite by response surface methodology, isotherm and kinetic studies, Nanotechnology for Environmental Engineering 3(1) (2018). doi: 10.1007/s41204-018-0046-y.

[85] Chatterjee S., Lee D.S., Lee M.W., Woo S.H., Enhanced molar sorption ratio for naphthalene through the impregnation of surfactant into chitosan hydrogel beads, Bioresource Technology 101(12) (2010) 4315-4321. doi: 10.1016/j.biortech.2010.01.062.

_____